Metallothionein dimerization evidenced by QD-based Förster resonance energy transfer and capillary electrophoresis

PAVELICOVÁ, K.; POMPEIANO VANÍČKOVÁ, L.; HADDAD, Y.; NEJDL, L.; ZÍTKA, J.; KOČIOVÁ, S.; MRAVEC, F.; VACULOVIČ, T.; MACKA, M.; VACULOVIČOVÁ, M.; ADAM, V.

International Journal of Biological Macromolecules
Volume 170, 15 February 2021, Pages 53-60

ISSN: 0141-8130

DOI: https://doi.org/10.1016/j.ijbiomac.2020.12.105

Accepted manuscript

Metallothionein dimerization evidenced by QD-based Förster resonance energy transfer and capillary electrophoresis

Kristyna Pavelicova[1,2], Lucie Vanickova[1,2], Yazan Haddad[1,2], Lukas Nejdl[1,2], Jan Zitka[1,2] Silvia Kociova[1,2], Filip Mravec[3], Tomas Vaculovic[4], Miroslav Macka[1,2,5], Marketa Vaculovicova[1,2*], Vojtech Adam[1,2*]

[1]*Department of Chemistry and Biochemistry, Mendel University in Brno, Zemedelska 1, CZ-613 00 Brno, Czech Republic*

[2]*Central European Institute of Technology, Brno University of Technology, Purkynova 123, CZ-612 00 Brno, Czech Republic*

[3] *Materials Research Centre, Faculty of Chemistry, Brno University of Technology, Purkynova 118, 612 00, Brno, Czech Republic*

[4]*Department of Chemistry, Faculty of Science, Masaryk University, Kamenice 753/5, CZ-625 00, Brno, Czech Republic*

[5]*School of Natural Sciences, Australian Centre for Research on Separation Science (ACROSS), University of Tasmania, Private Bag 75, Hobart 7001, Australia*

***Corresponding authors**

Vojtech Adam, Department of Chemistry and Biochemistry, Mendel University in Brno, Zemedelska 1, CZ-613 00 Brno, Czech Republic; E-mail: vojtech.adam@mendelu.cz; phone: +420-5-4513-3350; fax: +420-5-4521-2044

Marketa Vaculovicova, Department of Chemistry and Biochemistry, Mendel University in Brno, Zemedelska 1, CZ-613 00 Brno, Czech Republic; E-mail: marketa.ryvolova@seznam.cz; phone: +420-5-4513-3290; fax: +420-5-4521-2044

Abstract

Herein, we report a new simple and easy-to-use approach for the characterization of protein oligomerization based on fluorescence resonance energy transfer (FRET) and capillary electrophoresis with LED-induced detection. The FRET pair consisted of quantum dots (QDs) used as an emission tunable donor (emission wavelength of 450 nm) and a cyanine dye (Cy3), providing optimal optical properties as an acceptor. Nonoxidative dimerization of mammalian metallothionein (MT) was investigated using the donor and acceptor covalently conjugated to MT. The main functions of MTs within an organism include the transport and storage of essential metal ions and detoxification of toxic ions. Upon storage under aerobic conditions, MTs form dimers (as well as higher oligomers), which may play an essential role as mediators in oxidoreduction signaling pathways. Due to metal bridging by Cd^{2+} ions between molecules of metallothionein, the QDs and Cy3 were close enough, enabling a FRET signal. The FRET efficiency was calculated to be in the range of 11-77%. The formation of MT dimers in the presence of Cd^{2+} ions was confirmed by MALDI-MS analyses. Finally, the process of oligomerization resulting in FRET was monitored by CE, and oligomerization of MT was confirmed.

Keywords: FRET; Quantum dots; Oligomerization; Capillary electrophoresis

1. INTRODUCTION

Multiparametric fluorescence techniques utilizing molecular and nanoscale fluorescent reporters are widely used in life and material sciences because of their ease of use, suitability for *in vitro* and *in vivo* detection and imaging, sensitivity down to the single-molecule level, and nanoscale resolution. A common strategy for signal enhancement includes the use of multichromophore systems. However, the efficiency of such systems is predominantly controlled by dye−dye interactions. Depending on the orientation of the dye dipole moments, this interaction can lead to the formation of H-type dimers and aggregates. These types of aggregates are generally nonemissive or only very weakly emissive but can act as an energy channel *via* Förster/fluorescence resonance energy transfer (FRET), which is highly dependent on the distance between the acceptor and the donor fluorophores. An efficient transfer of energy from the donor to the acceptor occurs only when these groups are in close proximity to each other [1, 2]. The right choice of the FRET pair is essential. Fluorescent probes (i.e., organic dyes) are usually used in traditional FRET studies, but limitations (e.g., asymmetric emission spectra, insufficient long-term stability, and low resistance to photobleaching) can make successfully choosing the FRET pair a challenge. On the other hand, the optical properties of luminescent nanomaterials such as metal nanoclusters, organic-inorganic composites or quantum/carbon dots may enable overcoming some of these obstacles.

Quantum dots have unique optical properties, and these characteristics make them appealing as *in vivo* and *in vitro* fluorophores in a wide-ranging variety of applications. The ability of QDs to be conjugated to specific biomolecules and therefore target their interaction partners has led to applications in cellular labeling, deep-tissue imaging, and FRET [3-6]. The combination of FRET and fluorescent nanoparticles enabled us to develop a sensitive, selective and effective approach that can be flexibly modified and therefore tailored according to the analyte of interest. This approach represents a broad and elegant strategy for the investigation

of the structural properties of biomolecules (e.g., size or shape), dimerization, denaturation or intermolecular interactions.

From a biological point of view, protein dimerization (oligomerization) is responsible for certain vital functions since the failure of proper interaction may even lead to the development of disease. Among the proteins potentially associated with disease development, a small (6-7 kDa), nonenzymatic protein with a cysteine-rich structure (30%) and with high affinity to metals called metallothionein has been studied [7, 8]. This protein is composed of two domains, α and β, occurring as several tissue-specific isoforms (MT 1-4) [9]. The α domain (C-terminal) is more stable and can bind up to four divalent ions (Zn or Cd), while the β domain (N-terminal) can bind three metal ions and is more reactive [10, 11].

MT plays a critical role not only in the maintenance of homeostasis of essential metals such as zinc and copper but also in cell protection against the effects of toxic metals, primarily Cd, Hg and As [12]. Due to the reactivity of cysteine side chains, MTs can generate dimers [13]. Dimers can be formed either in an oxidative (e.g., NO) or nonoxidative (addition of excess Zn^{2+} and/or Cd^{2+}) manner [14]. The exact significance of MT dimerization in an oxidative manner is unclear. However, this process may be important for the function of metallothioneins as oxidoreductive mediators in signaling pathways. Therefore, dimerization mechanisms have been investigated, as they can help in understanding the role of oxidative stress or transport of toxic metals in the development of a number of diseases and disorders (e.g., cancer or neurological diseases including Parkinson´s disease and amyotrophic lateral sclerosis [7, 8, 13]). To study MT dimerization, numerous methods based on various physicochemical mechanisms have been suggested [15-21].

Despite these reports, the dimerization of MTs has not yet been fully explained. Therefore, it is necessary to find new simple, flexible, and easy-to-use methods to study the dimerization of metallothioneins. Herein, a new concept of investigation of protein dimerization is presented

based on the synergistic advantages of combining QD-based FRET with capillary electrophoresis with LED-induced fluorescence detection. Recent studies have shown that microfluidic chip electrophoresis is an effective tool in the early prediction of protein aggregation [22] and may have potential when combined with the FRET system for the analysis of biointeractions [23]. In contrast to microfluidic chip electrophoresis, the capillary electrophoresis-based approach presented here does not require complex and demanding chip fabrication and offers additional flexibility such as easier selection of capillary length, which may be beneficial for improved separation resolution. We demonstrate this new approach by using metallothionein to study its dimerization, which can be easily induced and reliably controlled by cadmium ion addition. Moreover, LED-induced fluorescence detection combined with simple UV irradiation-induced QD synthesis allows for flexible and variable modification of experimental parameters based on the application studied.

2. MATERIALS AND METHODS

2.1. Materials and reagents

The MT isoform (MT-1) from rabbit liver was obtained from Enzo Life Science, USA. Commercial cyanine 3 dye (Cy3) labeling kits, sodium borate, zinc acetate, cadmium acetate, sodium phosphate, mercaptosuccinic acid (MSA), isopropanol, *N*-ethyl-*N*′-(3-dimethylaminopropyl) carbodiimide hydrochloride (EDC) and *N*-hydroxysulfosuccinimide sodium salt (Sulfo-NHS) were purchased from Sigma-Aldrich (USA) in ACS quality. The stock solution of MT (1 mg/mL) was prepared with ultrapure water and stored in the dark at -20 °C. Ultrapure water, purified by a Milli-Q system (Czech Republic), was used for the preparation of all solutions.

2.2. Preparation of QDs

A suspension of ZnCd QDs was prepared by mixing stock solutions of 6 mM zinc acetate, 6 mM cadmium acetate, 20 mM sodium phosphate buffer (PB) pH 7.0 and 16 mM mercaptosuccinic acid (MSA). The resulting mixture with a typical molar ratio of 1:4:4:6 (Cd^{2+}:MSA:PB:Zn^{2+}) was exposed to UV irradiation for 5 minutes. The ZnCd QDs were precipitated with isopropanol and then isolated by centrifugation. Finally, the ZnCd QDs were suspended in PB (pH 7.2), and subsequently, the solution was sonicated for 2 minutes before use.

Determination of the photoluminescence quantum yield (PQY) of the ZnCd QDs was estimated according to our previous work [24], and the absolute value was calculated according to Equation 1:

$$\emptyset X = \emptyset ST \left(\frac{Gradx}{GradST}\right)\left(\frac{\eta^2 x}{\eta^2 ST}\right) \quad (1)$$

where the subscripts ST and X denote the standard and test, respectively, Ø is the fluorescence quantum yield (Ø ST = 0.54), and Grad is the gradient from the plot of integrated fluorescence intensity vs. absorbance (Grad ST = 80,000,000, and η is the refractive index of the solvent (1.333)).

2.3. QDs and Cy3 bioconjugation with MT

First, conjugation of ZnCd QDs with 0.1 mM MT-1 to form QDMT was carried out by a method using the coupling agents EDC and Sulfo-NHS according to a protocol published elsewhere [25]. Conjugation of Cy3 with MT-1 (Cy3MT) was carried out according to the manufacturer's protocol. A detailed description of the sample preparation is given in the Supplementary Information.

2.4. Zeta potential

The zeta potentials for MT-1, ZnCd QDs and their complexes were determined by dynamic light scattering using a Zetasizer Nano ZS instrument (Malvern-zetasizer Nano ZS, Malvern, UK). The zeta potential and size of the particles were measured by a dynamic light scattering technique using the same instrument. The parameters of particle size measurements were as follows: refractive index of the dispersive phase of 3.00 and 1.333 for the dispersive environment, adsorption coefficient of 10^{-3}, temperature of 25 °C, equilibration time of 120 s, and measurement angle of 173° backscatter. For the measurement, disposable ZEN 0040 cuvettes containing 50 μL of sample were used. The zeta potential measurement parameters such as temperature and equilibration time were the same as those in the particle size measurements. The calculations considered the diminishing particle concentration based on the Smoluchowski model, with an F(κa) parameter value of 1.50. For the measurement, disposable DTS1070 cuvettes were used. The measurements were performed under the automatic setting of attenuation and voltage selection. All measurements were carried out in triplicate.

2.5. MT dimerization

Dimers or higher oligomers of MTs were obtained by storing QDMT and Cy3MT mixtures (0.1 mM each mixed in a 1:1 ratio) in 20 mM PB (pH 9.3) in the presence of 0.5 mM Cd^{2+} at 8 °C under aerobic conditions for 1 week.

2.6. Homology model of the MT dimer

The 3D homology structure of rabbit MT1A was rendered from the Swiss-Model repository (UniProt ID P11957) [26]. The model was constructed using a rat homolog template (PDB ID 4MT2) [27], which has 85.3% sequence identity. Local quality estimates were lowest in the last 10 C-terminal residues, and their removal improved the QMEAN values from -3.58 to -

1.25 [28]. However, the aforementioned residues were not in direct contact with the second chain in the biological assembly. The MolProbity score and clash score of all atoms were 1.68 Å and zero, respectively [29]. The model was considered within acceptable parameters for further analysis. Superposition with rat homolog biological assembly (MT dimer) and visualization were performed in UCSF Chimera (version 1.10.2) [30].

2.7. Fluorescence analysis

Conjugate solutions (Cy3MT, QDMT and Cy3MTQDMT) were pipetted (100 µL) into a well microtiter plate (UV-transparent 96-well microtiter plate with flat bottom by CoStar (Corning, USA)), and emission spectra were recorded (λ_{Ex} = 390 nm and λ_{Em} = 420–750 nm). The fluorescence signal was acquired by a Tecan Infinite 200 M PRO multifunctional microplate reader (TECAN, Switzerland). Then, excitation or emission spectra were recorded using 2 nm steps and gain 100. In addition, the FRET efficiencies of the system by fluorescence analysis were calculated according to equation 1 based on the published protocol [4]:

$$E = 1 - \frac{F_{DA}}{F_D} \quad (1)$$

where F_{DA} is the donor fluorescence intensity in the presence of the acceptor and F_D is the donor fluorescence intensity in the absence of the acceptor.

2.8. CE analysis of FRET

Monitoring of the FRET signal between MT conjugates was performed using a Beckman Coulter CE instrument (P/ACE 5500, USA) equipped with a light-emitting diode (390 nm) as an excitation source and a bandpass emission filter (607 ± 20 nm). Separations were performed in an uncoated fused-silica capillary (Polymicro Technologies, USA) with an internal diameter of 75 µm and external diameter of 375 µm. The total length of the capillary was 46.5 cm, and the effective length to the detection window was 36.0 cm. The capillary was flushed with 0.1

M NaOH for 5 min and with background electrolyte (sodium borate buffer with 5% ethanol, pH 10) for 15 min prior to the first use. Before each run, the capillary was rinsed for 120 s with background electrolyte (BGE). The sample was injected hydrodynamically at a pressure of 1 psi for 4 s. The separation voltage was 15 kV.

2.9 FRET analysis using lifetime detection

The Förster resonance energy transfer in a given sample was determined using a MicroTime 200 fluorescence microscope (Picoquant GmbH, Germany). The excitation source was a laser diode head LDH-375 with a wavelength of 375 nm. Donor emission was monitored through a 440/40 emission filter (Chroma Inc. USA) and scanned with a SPCM-AQRH detector (Excelitas Technologies, USA) with a HydraHarp 400 timer. The lifetime of the donor and donor in the presence of an acceptor was determined.

2.10. Matrix-Assisted Laser Desorption/Ionization Time-of-Flight Mass Spectrometric analyses

Characterization of commercial MT-1A samples was carried out by MALDI-MS to ensure protein purity (**Fig. S1A**). Samples of MT-1A (1 µL, 0.016 mM) and MT-1A with Cd^{2+} (0.5 mM) were pipetted on a matrix-assisted laser desorption/ionization (MALDI) stainless steel target (Bruker Daltonik GmbH, Bremen, Germany). After drying at room temperature, 1 µL of matrix solution (10 mg of 2,5-dihydroxybenzoic acid in 1 mL of 3:7 acetonitrile/water and 0.1% trifluoracetic acid) was added to each spot, and the target was left to dry at ambient temperature (25 °C). MT-1A dimer formation was further confirmed by MALDI time-of-flight mass spectrometry (TOF-MS) analyses using an ultrafleXtreme instrument (Bruker Daltonik GmbH, Bremen, Germany) equipped with a laser (operating at a wavelength of 355 nm, with an accelerating voltage of 25 kV, maximum energy of 43.2 µJ, and repetition rate of 2000 Hz)

in linear positive ion mode. External calibration using a protein standard mixture I and II (Bruker Daltonik, Bremen, Germany) was applied in the range of *m*/*z* 1–30 kDa. A total of 3000 spectra were summed for each spot using the random walk raster pattern, with no evaluation criteria, and were analyzed with Flex Analysis software (Version 3.4).

2.11. Capillary Electrophoresis Inductively Coupled Plasma Mass Spectrometric analysis

The metal content of commercial MT-1A was monitored by CE-ICP-MS. A detailed description is given in the supplementary materials, and the resulting electropherogram confirming the supplier´s information about the chelation of Zn ions is shown in **Fig. S1B**.

3. RESULTS AND DISCUSSION

Current interest in the biological functions of proteins and their possible relation to disease development has led to advances in multidisciplinary fields. In addition to conventional methods of analytical chemistry and/or biochemistry, comparative modeling (*i.e.*, homology modeling) has been used to study 3D protein structures *in silico*, particularly in the absence of a known crystal structure. The combination of 3D modeling with analytical and biochemical evidence of the calculated findings is of great interest.

3.1. Calculated structure of the MT dimer

Regarding metallothionein dimerization, the closest known homolog 3D structure to rabbit MT1A presented in the literature was the rat MT2 3D structure (PDB ID 4MT2) published by Braun et al. [27]. Their findings confirmed that the rat MT2 dimer had identical molecular architectures from both X-ray crystallography and NMR analyses. In contrast to previous hypotheses about the flexibility of MT, their findings were the first to suggest a stable architecture of the MT dimer in solution. The flexibility, however, allows accommodating different atomic sizes of metals without substantial changes in the folding of the protein. Therefore, this model was ideally suited to study the nonoxidative form of the rabbit MT1A dimer. Briefly, the homology model of the rabbit MT1A dimer shows a distinct AQG loop (residues 45–47) of the alpha domain embedded in the cleft between the alpha and beta domains of the other chain (**Fig. 1A**). The Q46 residue in particular, also conserved in rats, is deeply

embedded with direct contact facing the K31, C21 and C24 residues of the opposing chain. Other contacts of the side chains involve T27, T42 and K43 since the cysteine chains are oriented inwards towards the metal ions. A sodium atom and two molecules of water are present in crystalline form in the space adjacent to the/a TKC helix (residues 42–44) in the rat homolog dimer. Despite the absence of atomic clashes in our model, we were not able to detect direct H-bonds between the two chains. However, the interaction interface is rich with polar and charged residues in close proximity. This model suggests a dimer structure where the cysteine residues are fully loaded with metal ions and the dimer is stabilized by polar and van der Waals interactions. Further molecular dynamics simulations are required to identify the interactions leading to dimerization. We believe that this assessment is a great challenge for several reasons. First, the protonation states of the cysteine residues are believed to be dynamic. Second, Cd ions have a more complex electronic structure than Zn ions, which is not yet represented in the force fields of classical molecular dynamics. Researchers often compromise accuracy by substituting Cd with Zn in their computations. Finally, while the quantum mechanics/molecular mechanics (QM/MM) approach is a standard way of solving the previously mentioned peculiarities, the MT dimer is considered a relatively large system for such computations.

Structure identified by structural methods

In contrast, sophisticated methods of structural chemistry (i.e., nuclear magnetic resonance spectroscopy) by Zangger et al. report oxidative head-to-head [16] dimerization, as shown in **Fig. 1B**. Their study of mouse and rabbit MTs elucidated a tight interaction between the alpha domains of two MT chains in the presence of oxidative stress. Surprisingly, despite the hypothesized flexibility and reactivity of the MT beta domain, their findings showed that oxidative dimerization did not affect the mobility of the metal ions in either domain.

Even though structural methods are able to provide an enormous amount of detail and valuable information, little is known about the frequency of either oxidative or nonoxidative dimerization *in vitro* and *in vivo*. Therefore, the development of a simple, user-friendly, fluorescence-based approach is very important for both analytical- and microscopy-based studies of MT dimerization. Therefore, we proceeded to develop such a method.

Dimerization monitored by FRET-CE

Fluorescence spectroscopy in combination with separation techniques such as capillary electrophoresis offers the capability of investigating intermolecular interactions. Moreover, the basic principles of the FRET phenomenon offer insight into the structural behavior of the studied molecules. It is known that the optimal FRET effect occurs if the distance between the fluorophores is approximately 8 nm [31]. Based on this fact, a number of molecular interactions may be effectively studied, including denaturation, dimerization or even intermolecular interactions. Furthermore, the electrophoretic separation of various components present in the reaction mixture enables us to distinguish the FRET occurring between fluorophores randomly present at the optimal distance from the FRET occurring between fluorophores in physicochemical interactions, as is the case for dimers. MT was chosen in this study due to the tunable *in vitro* dimerization easily controlled by the addition of Cd ions. Due to the presence of 8 lysine molecules in the MT sequence, multiple labeling may occur and potentially complicate the process; however, as shown below, the labeling ratio is significantly lower than expected.

As predicted in our homology model, all lysine molecules were facing towards the solution, except for Lys31, which is solvent-accessible. Lysine molecules are one of the longest amino acids, with a flexible side chain length of nearly 6 Å. We assume that the interaction of lysine molecules with cyanine dye and QDs would not affect the internal conformation of MT. The bioconjugates were prepared separately to decrease the likelihood of forming QD-only or Cy3-

only dimers. The main advantage of the proposed method of combining FRET with separation by CE is the verification of the presence of a stable linkage. In contrast, in steady-state fluorescence spectroscopy, FRET may occur just by random proximity of protein molecules (statistically) even without dimerization.

3.2. Characterization of QDs and cyanine dye

Successful FRET-based investigations depend on the correct selection of fluorophores. In this study, quantum dots were used as the donor fluorophore, and the dye Cy3 was employed as the acceptor. The main advantage of this selected donor-acceptor pair is that QDs are fluorescent tags yielding relatively broad absorption spectra in the UV region; therefore, different QDs (having different emission wavelengths) can be simultaneously excited by one excitation light source. Moreover, the emission wavelength tenability simplifies the selection of the acceptor fluorophore in the FRET pair. Finally, the synthesis procedure is very simple and elegant, involving only 5 minutes of UV light irradiation of the precursors.

As the first step, the absorption and emission spectra of ZnCd QDs and Cy3 dye were measured (**Fig. S2**). These spectra showed that the absorption and emission maxima of ZnCd QDs were 350 nm and 450 nm, respectively (**Fig. S2A**), while for the Cy3 dye, the wavelengths were 550 nm and 570 nm (**Fig. S2B**). It was clear that the donor emission spectrum and the acceptor absorption spectrum have the necessary spectral overlap required for a high-yield FRET system (**Fig. S2C**). Moreover, the PQY of the ZnCd QDs was 47%. Subsequently, the probes were conjugated with metallothionein isoform MT-1. ZnCd QDs were conjugated with MTs by covalent bonding using the coupling agents EDC and Sulfo-NHS according to a previously published protocol [25]. The conjugation of MTs with Cy3 was carried out according to the manufacturer's protocol. It should be noted that the size of the ZnCd QDs was 2.2 nm, as this size offers the desired emission. The measured zeta potential for the ZnCd QDs was -26.9 mV,

which means that the QDs are stable and do not agglomerate. Furthermore, the zeta potential observed for the QDMT (-18.2 mV) conjugate was less negative than that in the case of bare ZnCd QDs.

3.3. MT conjugates analyzed by fluorescence spectroscopy

Notwithstanding the above outlined power of combining FRET with CE, steady-state fluorescence spectroscopy is the first method of choice because it is relatively simple yet capable of evaluating the proper selection of FRET pair partners as well as the effectiveness of energy transfer. Therefore, the optical properties of QDMT, Cy3MT, and their conjugate (Cy3MTQDMT) were first studied by fluorescence spectroscopy. As illustrated in **Fig. 2**, the typical emission spectra of all conjugates exhibit the FRET signal, here shown for the Cy3MTQDMT sample (λ_{ex}=390 nm, λ_{em}=570 nm). To validate the suitability of the individual fluorophores, the performance of the QD-Cy3 pair was compared to that of the QD-Cy3.5 pair. However, the FRET efficiency (detailed in the Fluorescence analysis section) was significantly lower with Cy 3.5 than with Cy3, as shown in **Fig. S3**.

Fig. 3 shows the change in fluorescence intensity with gradually increasing Cy3MT concentration while keeping the QDMT concentration in the mixture constant. After background correction, the fluorescence intensity of the acceptor was obtained by subtracting the Cy3MT signal from each spectrum. As the amount of acceptor (Cy3MT) increased, the fluorescence intensity of the donor (QDMT) gradually decreased, while the fluorescence intensity of the acceptor increased. The FRET efficiency of the system by fluorescence spectroscopy calculated according to a published protocol [4] was in the range of 11-77% (**Fig. S4**). To verify our approach, the lifetime of particular FRET partners was measured, as shown in **Fig. S5**. The FRET efficiency was calculated to be 40%. In comparison, the same sample

measured by capillary electrophoresis exhibited an efficiency of 77%; however, this parameter is highly dependent on the instrumental setup.

The Förster critical radius R_0 of the donor-acceptor pair was also calculated using equation 3:

$$R_0 = \frac{9000 ln10 \kappa^2 \phi_D}{128\pi^5 n^4 N_A} \int_0^\infty \frac{F_D(\lambda)\varepsilon_A(\lambda)d\lambda}{\lambda^4} \quad (3)$$

where n is the refractive index of the medium, κ^2 is the orientation factor, Φ_D is the fluorescence quantum yield, $F_D(\lambda)$ is the normalized fluorescence spectrum of the donor, $\varepsilon_A(\lambda)$ is the molar absorptivity of the acceptor and λ is the wavelength in cm.

The Förster radius for paired QDs with Cy3 was estimated as $R_0 = 5.6$ nm.

3.4. Study of MT-conjugates by CE

The stoichiometry of the interaction between nanoparticles and proteins is of particular importance in the context of this work. To investigate the stoichiometry, QDMT conjugates were prepared by conjugating MT at a constant concentration while increasing the concentration of QDs (**Table S1**), and the conjugates were subsequently analyzed by CE-UV/Vis. The migration times of individual components (**Fig. S6A**) were used to find the point at which the maximum number of available interaction sites was saturated (**Fig. S6B**). The approach taken by Hlavacek et al. was used [32], and a plot demonstrating the QD-protein interaction was constructed (**Fig. S6B**). It was calculated that on average, 3.7 protein molecules are conjugated to one QD particle.

Thereafter, MTs labeled by QDs as the donor moieties, MTs labeled by Cy3 as the acceptor fluorophore, a mixture of labeled MTs (Cy3MTQDMT) and a mixture of labeled MTs with Cd^{2+} addition (Cy3MTQDMTCd) were all studied by CE with LED-induced fluorescence detection. It should be emphasized that the reason for utilization of a separation technique is quite simple. In steady-state fluorescence spectroscopy, FRET can occur not only between species that are physically connected but also between species, which are in appropriate proximity just by chance within statistical probability. Separation of the mixture ensures that

the donor and acceptor are linked with a sufficiently strong interaction and separates the detected sample components (the zones migrating through the detector) from the monomers potentially present in the injected sample mixture. At the same time, the detection of a pure FRET signal (fluorescence resulting only from FRET) eliminates the detection of dimers resulting from dimerization of the same species (Cy3MTCy3MT or QDMTQDMT) because these homodimers would not be detected as only FRET fluorescence is detected; nonspecific fluorescence at other wavelengths is suppressed owing to the selection of optical filters. In other words, Cy3MTCy3MT could not be excited, and the emission of QDMTQDMT could not be detected.

The system allowed flexible selection of the excitation wavelength according to the desired fluorophores. It can be clearly seen (**Fig. 4**) that both Cy3MT and QDMT provide very low signals (red and yellow traces). This is because an excitation wavelength of 390 nm was used. This wavelength is optimal for excitation of QDs, but the emission arrangement (emission bandpass filter with a central wavelength of 607 nm) prevented the detection of QD emission. On the other hand, this emission arrangement would be optimal for monitoring Cy3 emission; however, the excitation of Cy3 by 390 nm is very inefficient (the optimal excitation wavelength of Cy3 is 550 nm). This weak signal is treated as a background signal. When the interaction between the conjugates Cy3MT and QDMT takes place, FRET occurs between Cy3 and QD; therefore, a signal was obtained for the mixture of Cy3MT and QDMT (green trace). As explained in detail above, the separation ensures that noninteracting species do not influence the detection. Then, the FRET signal significantly increased after the addition of Cd ions (brown trace), which demonstrated increased dimer formation under the given conditions. The same migration times of the major peaks in the green and brown traces are in agreement with the fact that these are the same species (Cy3MTQDMT), differing only in quantity. As the rate of dimerization was enhanced (brown trace) compared to that of naturally occurring

dimerization (green trace), the signal corresponding to dimer formation increased. Therefore, it can be concluded that the proposed method is suitable for investigating the kinetics as well as the behavior under various environmental conditions (e.g., oxidative and/or nonoxidative dimerization).

It should be noted that the somewhat higher noise is caused by the generally well-known relatively low power of UV LEDs (compared to laser excitation) and by suboptimal coupling between the excitation source and light-guiding optical fiber [33].

The electrophoretic mobilities calculated for the different species are summarized in **Table 1**. These results show that the quantum dots as well as the Cy3 dye are significantly negatively charged anionic species, as their mobilities are -37.3 and -26.7×10^{-9} $m^2 \cdot V^{-1} \cdot s^{-1}$, respectively. On the other hand, MT-1 is negatively charged to a much lower degree (-7.1×10^{-9} $m^2 \cdot V^{-1} \cdot s^{-1}$). Furthermore, dimerization by Cd addition leads to a negligible decrease in electrophoretic mobility (-9.1×10^{-9} $m^2 \cdot V^{-1} \cdot s^{-1}$). Such a small change would hardly be noticeable by common photometric detection under simple separation conditions. However, the increase in the fluorescence FRET signal is very significant (250%). Importantly, when dimerization was facilitated by Cd ions, the change in electrophoretic mobility was in a similar range (from -9.1×10^{-9} $m^2 \cdot V^{-1} \cdot s^{-1}$ to -13.0×10^{-9} $m^2 \cdot V^{-1} \cdot s^{-1}$); however, the increase in the signal intensity was even more pronounced (500%).

3.5. MALDI-TOF-MS analyses of MT oligomerization

To further confirm the oligomerization of MT-1 in the presence of excess Cd ions, the MALDI-TOF-MS technique was used. The data shown in **Fig. 5** confirm that dimerization caused by Cd addition occurred and that metal bridges were formed. The relative intensity of the signal of the MT dimer (m/z 12 458.897) increased significantly in the MT sample with Cd addition after 1 week of storage at 8 °C under aerobic conditions. The MALDI-TOF-MS method was

previously applied for the characterization of the structures of different MT isoforms [34] and their oligomeric formation. Compared to MALDI mass spectrometric analysis, which may be problematic in terms of precise quantification, the FRET-CE method developed here provides more reliable results, especially when the light source coupling efficiency is optimized.

Finally, MT dimerization under various conditions was investigated by the developed method to demonstrate its applicability. As known from the literature, two types of MT dimerization are known. In the first process, oxidative bonds result in the formation of intermolecular disulfidic bonds[16], while the in the second process, nonoxidative bonds are triggered by Cd addition and result in the formation of inter- and intramolecular metal bridges [35-37].

As shown in **Fig. 6**, the MT solution stored under aerobic conditions (schematically shown in **Fig. 6 left**) provided a significantly stronger fluorescence FRET signal than MT in the presence of $NaBH_4$. It is believed that $NaBH_4$ addition caused the reduction of disulfidic bonds, leading to a significant decrease in the fluorescence FRET signal. On the other hand, MT in the presence of Cd ions exhibited a higher intensity FRET signal (**Fig. 6 middle**), which suggests increased dimer formation induced by metal bridge formation (**Fig. 6 right**). Even though capillary electrophoresis has already proven its outstanding capabilities not only in protein quaternary structure investigations but also in MT dimerization research [38, 39], additional FRET modalities may provide (under finely optimized conditions) further information on the spatial arrangement of protein molecules.

4. CONCLUSIONS

The method proposed here based on the synergistic power of FRET and CE can serve as a flexible and simple tool to study the dimerization of MTs and the conditions under which they occur. Moreover, LED-induced fluorescence detection appears to be beneficial for dimerization investigation by CE; however, the geometrical arrangement, primarily LED-

optical fiber pigtailing, has to be adjusted to decrease the noise and improve the signal-to-noise ratio.

In this study, while dimerization enhanced by Cd ion addition was employed, it is important to stress that other conditions may also lead to dimer formation, so the approach developed here has a more general applicability. Additionally, the desired FRET pair properties can be easily tuned by adjusting the size of the QD used. Finally, several different "QD-dye" pairs can be excited by the same wavelength. Therefore, multiplexed dimerization assays can be envisioned. In addition, the aim of the study was to demonstrate the overall approach, which can be flexibly adopted for the investigation of other proteins with a lower number of lysine residues. Alternatively, mutated proteins could be prepared by molecular biology methods, selectively replacing lysine residues in specific positions. By such an approach, even the structural arrangement of protein dimers (spatial orientation of monomers) could be elucidated, considering the distance required for FRET to occur.

Conflict of interest

Authors declare no conflict of interest.

Acknowledgments

This research was funded by the European Research Council (ERC) under the European Union´s Horizon 2020 research and innovation program (grant agreement no. 759585) and by the internal grant agency MENDELU IGA grant no. IP_025/2019, DFG-GACR (reg. no. 19-13766 J) project CEITEC 2020 (LQ1601) with financial support from the Ministry of Education, Youth and Sports of the Czech Republic under National Sustainability Programme II. LV was supported by project 6SA17676, which received funding from the European Union's Horizon 2020 research and innovation program under the Marie Skłodowska-Curie

and is cofinanced by the South Moravian Region under grant agreement no. 665860. The authors confirm that the content of this work reflects only the authors' view and that the EU is not responsible for any use that may be made of the information that it contains. M.M. acknowledges his Australian Research Council (ARC) Future Fellowship Level 3 (FT120100559).

Captions for Figures

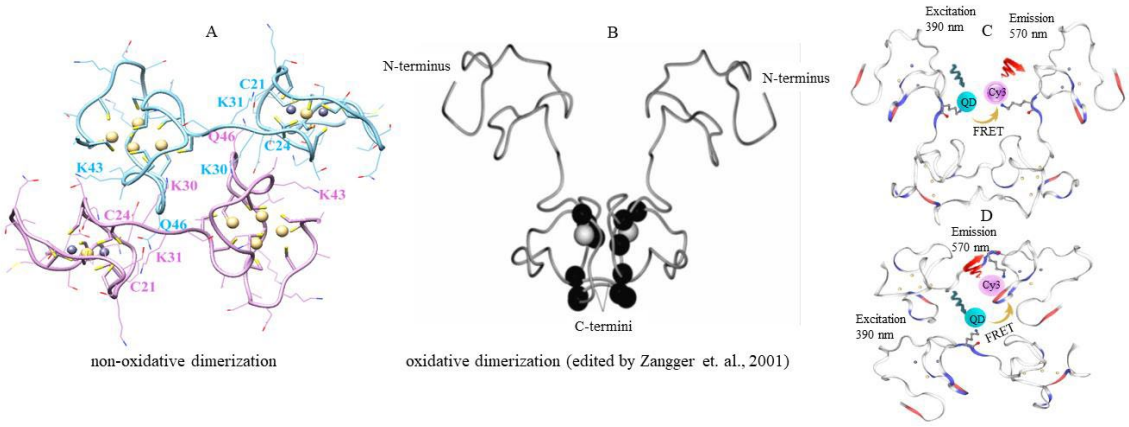

Figure 1

(**A**) Nonoxidative homology model of the rabbit MT1A dimer structure based on a85n .3% identity rat MT homolog. The polypeptide chains are shown in blue and pink ribbons. Cysteine residues are shown as sticks, while other amino acids are shown as wires. Five cadmium and two zinc atoms per chain are shown in gold and gray, respectively. Sodium atoms are not shown. (B) Previously published by Zangger et al. [16], reused based on the STM Permissions Guidelines, and schematic representation of FRET analysis of (**C**) nonoxidative and (**D**) oxidative dimerization of MTs (labeled by Cy3 and QDs).

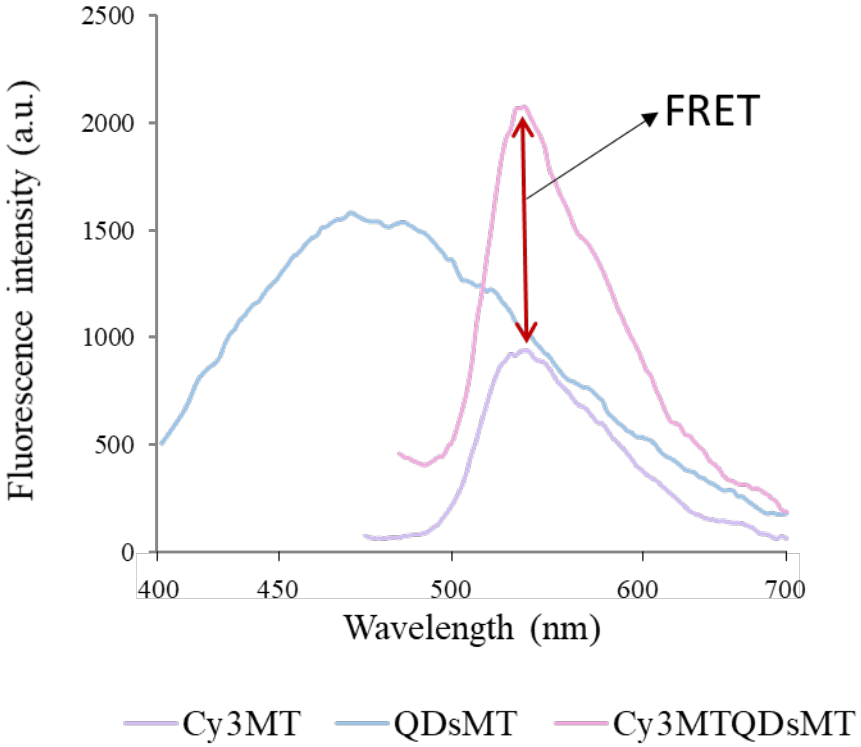

Figure 2

Emission spectra of Cy3MT, QDMT and Cy3MTQDMT conjugates. Excitation wavelength 390 nm. For other conditions, see the Experimental section.

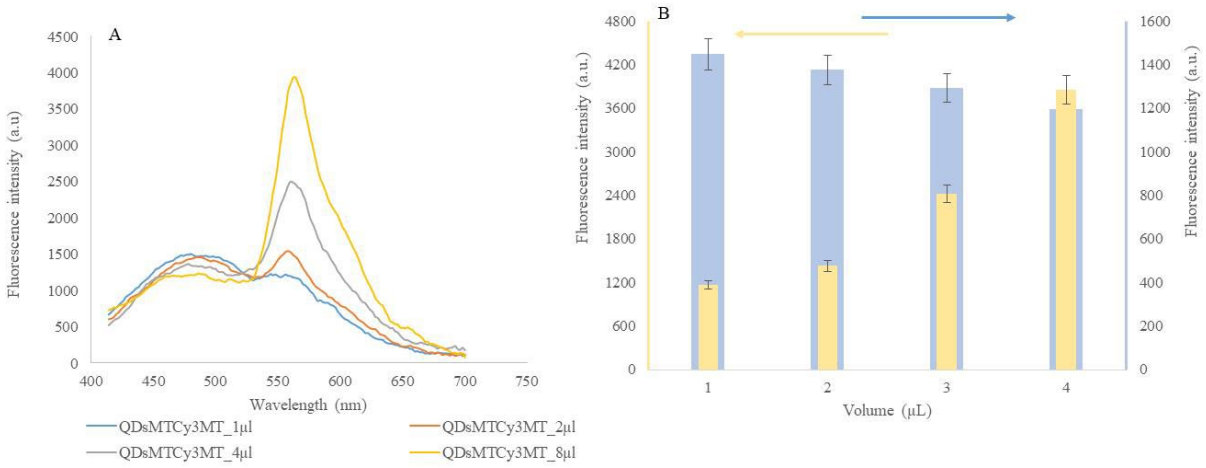

Figure 3

(**A**) Emission spectra of Cy3MTQDMT conjugates with different volumes (1, 2, 4 and 8 µL of Cy3MT acceptor). The fluorescence intensity of Cy3MT was obtained by subtracting the Cy3 signal from each spectrum and correcting for the background. (**B**) Signal intensity dependence on the amount of Cy3MT at an emission wavelength of 570 nm. While the signal intensity of the acceptor (Cy3MT) was increased (as demonstrated in yellow), the signal intensity of the donor (QDMT) was decreased (as demonstrated in blue).

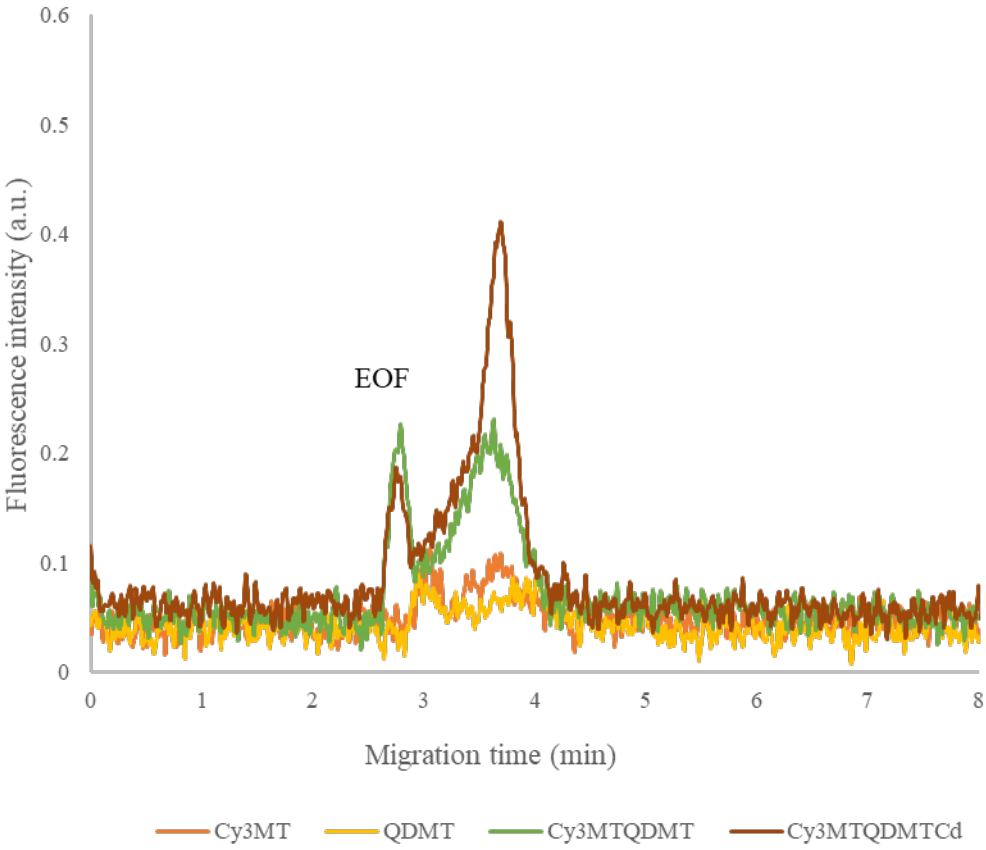

Figure 4

Electropherograms of samples of MTs without Cd^{2+} addition analyzed immediately and samples of MTs with Cd^{2+} addition after 1 week of storage.

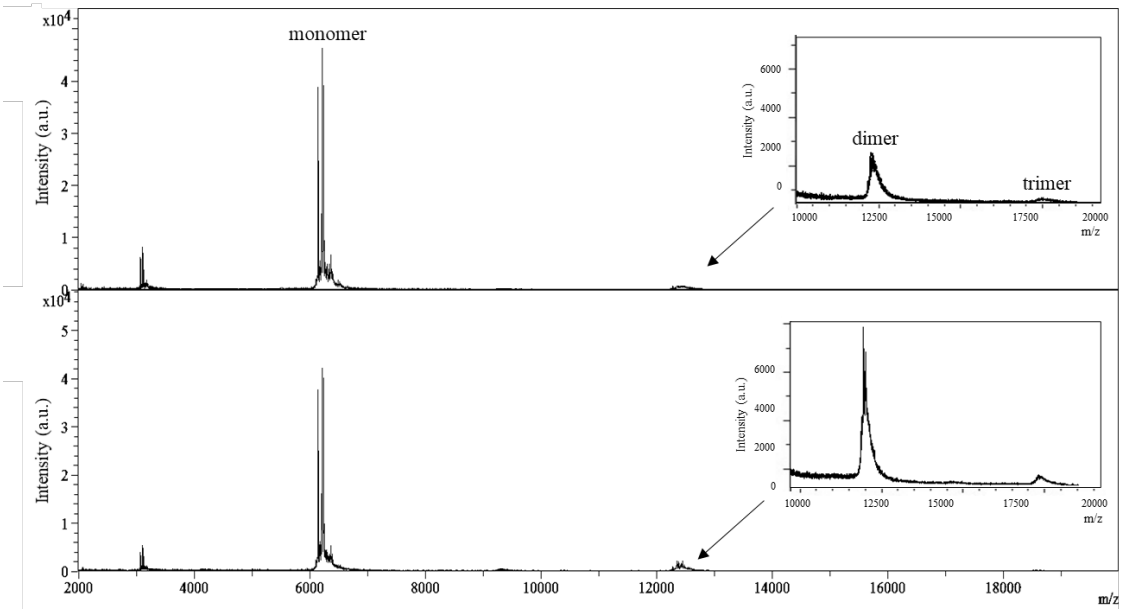

Figure 5

MALDI-TOF mass spectra of MT-1. Sample of MT-1 standard (top) and sample of MT-1 with added Cd^{2+} after 1 week of storage at 8 °C under aerobic conditions (bottom).

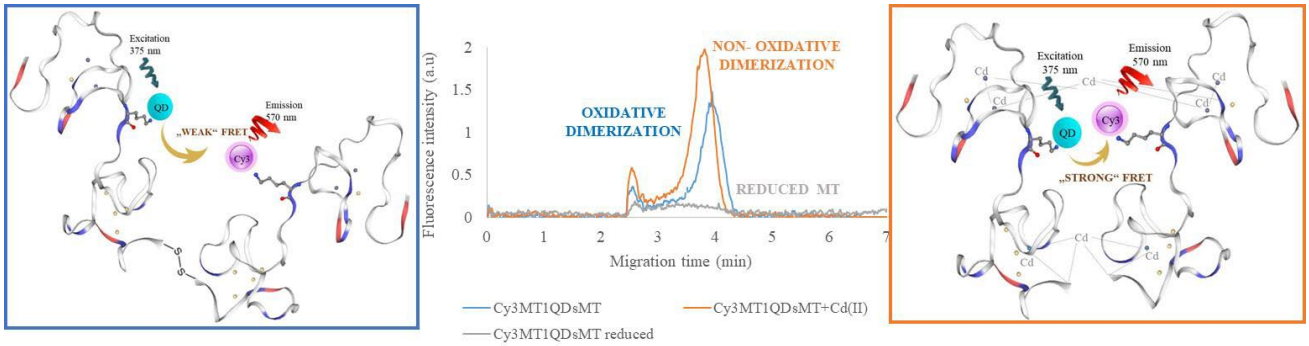

Figure 6

Comparison of oxidative and nonoxidative dimerization. Schematic representation of oxidative dimerization (left), FRET CE of Cy3MT1QDMT1 (middle): dimerized under aerobic conditions (blue), after the addition of Cd(II) to induce nonoxidative dimerization (orange), after the addition of BH4 to reduce the dimeric structure (gray), and schematic representation of nonoxidative dimerization and metal bridge formation (right).

Table 1 *Electrophoretic mobilities (10^{-9} $m^2 \cdot V^{-1} \cdot s^{-1}$)*

Species	Mobility
MT-1	-7.1
MT1 + 0.5 mM Cd^{2+}	-9.1
QDMT	-23
Cy3MT	-14.3
	-20.3
Cy3MTQDMT	-11
Cy3MTQDMTCd	-13
QDs	-37.3
Cy3	-26.7

References

[1] Y. Zhang, T.H. Wang, Theranostics, 2 (2012) 631-654.
[2] Y. Choi, L. Kotthoff, L. Olejko, U. Resch-Genger, I. Bald, ACS Appl. Mater. Interfaces, 10 (2018) 23295-23302.
[3] X.J. Zhang, Y. Hu, X.T. Yang, Y.Y. Tang, S.Y. Han, A. Kang, H.S. Deng, Y.M. Chi, D. Zhu, Y. Lu, Biosens. Bioelectron., 138 (2019) 1-13.
[4] Y.Q. Li, J.H. Wang, H.L. Zhang, J. Yang, L.Y. Guan, H. Chen, Q.M. Luo, Y.D. Zhao, Biosens. Bioelectron., 25 (2010) 1283-1289.
[5] M. Stanisavljevic, S. Krizkova, M. Vaculovicova, R. Kizek, V. Adam, Biosens. Bioelectron., 74 (2015) 562-574.
[6] K.K. Jain, The handbook of nanomedicine, 2nd ed., Humana Press., New York, 2012.
[7] S. Krizkova, M. Kepinska, G. Emri, T. Eckschlager, M. Stiborova, P. Pokorna, Z. Heger, V. Adam, Pharmacol. Ther., 183 (2018) 90-117.
[8] T. Eckschlager, V. Adam, J. Hrabeta, K. Figova, R. Kizek, Curr. Protein Pept. Sci., 10 (2009) 360-375.
[9] M.A.R. Merlos, A.M. Jimenez Jimenez, Y. Haddad, K. Bodoor, P. Adam, S. Krizkova, Z. Heger, V. Adam, Drug Resist. Updates, in press (2020).
[10] M. Ryvolova, V. Adam, R. Kizek, J. Chromatogr. A, 1226 (2012) 31-42.
[11] B. Ruttkay-Nedecky, L. Nejdl, J. Gumulec, O. Zitka, M. Masarik, T. Eckschlager, M. Stiborova, V. Adam, R. Kizek, Int. J. Mol. Sci., 14 (2013) 6044-6066.
[12] R. Garla, B.P. Mohanty, R. Ganger, M. Sudarshan, M.P. Bansal, M.L. Garg, Biometals, 26 (2013) 887-896.
[13] P. Adam, S. Krizkova, Z. Heger, P. Babula, V. Pekarik, M. Vaculovicova, C.M. Gomez, R. Kizek, V. Adam, J. Alzheimers Dis., 51 (2016) 637-656.
[14] S. Krizkova, M. Masarik, T. Eckschlager, V. Adam, R. Kizek, J. Chromatogr. A, 1217 (2010) 7966-7971.
[15] V. Sanz-Nebot, B. Andon, J. Barbosa, J. Chromatogr. B, 796 (2003) 379-393.
[16] K. Zangger, G. Shen, G. Oz, J.D. Otvos, I.M. Armitage, Biochem. J., 359 (2001) 353-360.
[17] M. Ryvolova, D. Hynek, H. Skutkova, V. Adam, I. Provaznik, R. Kizek, Electrophoresis, 33 (2012) 270-279.
[18] C.L. Tenorio-Daussat, M.C.M. Resende, R.L. Ziolli, R.A. Hauser-Davis, D. Schaumloffel, T.D. Saint'Pierre, Talanta, 120 (2014) 491-497.
[19] E. Guszpit, P. Kopel, S. Krizkova, H. Milnerowicz, Colloid Surf. B-Biointerfaces, 170 (2018) 447-453.
[20] V. Adam, I. Fabrik, T. Eckschlager, M. Stiborova, L. Trnkova, R. Kizek, TRAC-Trends Anal. Chem., 29 (2010) 409-418.
[21] O. Zitka, S. Krizkova, D. Huska, V. Adam, J. Hubalek, T. Eckschlager, R. Kizek, Electrophoresis, 32 (2011) 857-860.
[22] S.Y. Yu, J.D. Xu, K.J. Huang, J. Chen, J.Y. Duan, Y.Q. Xu, H. Qing, L.N. Geng, Y.L. Deng, Anal. Methods, 8 (2016) 8306-8313.
[23] Y. Lu, S.Y. Yu, F.M. Lin, F.K. Lin, X.C. Zhao, L.Q. Wu, Y.F. Miao, H.J. Li, Y.L. Deng, L.N. Geng, Analyst, 142 (2017) 4257-4264.
[24] L. Nejdl, K. Zemankova, M. Havlikova, M. Buresova, D. Hynek, K. Xhaxhiu, F. Mravec, M. Matouskova, V. Adam, M. Ferus, J. Kapus, M. Vaculovicova, Nanomaterials, 10 (2020) 1-14.

[25] M. Pereira, E. Lai, J. Nanobiotech., 6 (2008) 1-10.
[26] T. Schwede, J. Kopp, N. Guex, M.C. Peitsch, Nucleic Acids Res., 31 (2003) 3381-3385.
[27] W. Braun, M. Vasak, A.H. Robbins, C.D. Stout, G. Wagner, J.H.R. Kagi, K. Wuthrich, Proc. Natl. Acad. Sci. U. S. A., 89 (1992) 10124-10128.
[28] P. Benkert, M. Kunzli, T. Schwede, Nucleic Acids Res., 37 (2009) W510-W514.
[29] V.B. Chen, W.B. Arendall, J.J. Headd, D.A. Keedy, R.M. Immormino, G.J. Kapral, L.W. Murray, J.S. Richardson, D.C. Richardson, Acta Crystallogr. Sect. D-Struct. Biol., 66 (2010) 12-21.
[30] E.F. Pettersen, T.D. Goddard, C.C. Huang, G.S. Couch, D.M. Greenblatt, E.C. Meng, T.E. Ferrin, J. Comput. Chem., 25 (2004) 1605-1612.
[31] R. Freeman, J. Girsh, I. Willner, ACS Appl. Mater. Interfaces, 5 (2013) 2815-2834.
[32] A. Hlavacek, P. Skladal, Electrophoresis, 33 (2012) 1427-1430.
[33] P. Smejkal, A. Szekrenyes, M. Ryvolova, F. Foret, A. Guttman, F. Bek, M. Macka, Electrophoresis, 31 (2010) 3783-3786.
[34] C.P. Mercogliano, D.J. DeRosier, J. Struct. Biol., 160 (2007) 70-82.
[35] P. Palumaa, E.A. Mackay, M. Vasak, Biochemistry, 31 (1992) 2181-2186.
[36] P. Palumaa, M. Vaher, Ann. Clin. Lab. Sci., 26 (1996) 264-268.
[37] K. Zangger, I.M. Armitage, J. Inorg. Biochem., 88 (2002) 135-143.
[38] T.W. Wilhelmsen, P.A. Olsvik, R.A. Andersen, Talanta, 57 (2002) 707-720.
[39] T.W. Wilhelmsen, P.A. Olsvik, B.H. Hansen, R.A. Andersen, J. Chromatogr. A, 979 (2002) 249-254.